NASA Technical Memorandum 100268

Numerical and Analytical Study of Fluid Dynamic Forces in Seals and Bearings

L.T. Tam and A.J. Przekwas
CHAM of North America, Inc.
Huntsville, Alabama

A. Muszynska
Bentley Rotor Dynamics Research Corporation
Minden, Nevada

R.C. Hendricks
Lewis Research Center
Cleveland, Ohio

M.J. Braun
University of Akron
Akron, Ohio

R.L. Mullen
Case Western Reserve University
Cleveland, Ohio

Prepared for the
11th Biennial Design Engineering Conference on Vibration and Noise
sponsored by the American Society of Mechanical Engineers
Boston, Massachusetts, September 27–30, 1987

NASA

NUMERICAL AND ANALYTICAL STUDY OF FLUID DYNAMIC FORCES IN SEALS AND BEARINGS

L.T. Tam and A.J. Przekwas
CHAM of North America, Inc.
Huntsville, Alabama 35816

A. Muszynska
Bently Rotor Dynamics Research Corporation
Minden, Nevada 89423

R.C. Hendricks
National Aeronautics and Space Administration
Lewis Research Center
Cleveland, Ohio 44135

M.J. Braun
University of Akron
Akron, Ohio 44325

R.L. Mullen
Case Western Reserve University
Cleveland, Ohio 44106

SUMMARY

A numerical model based on a transformed, conservative form of the three-dimensional Navier-Stokes equation and an analytical model based on "lumped" fluid parameters are presented and compared with studies of modeled rotor bearing/seal systems. The rotor destabilizing factors are related to the rotative character of the flow field. It is shown that these destabilizing factors can be reduced through a decrease in the fluid average circumferential velocity. However, the rotative character of the flow field is a complex three-dimensional system with bifurcated secondary flow patterns that significantly alter the fluid circumferential velocity. By transforming the Navier-Stokes equations to those for a rotating observer and using the numerical code PHOENICS-84 with a nonorthogonal body-fitted grid, several numerical experiments were carried out to demonstrate the character of this complex flow field. In general, fluid injection and/or preswirl of the flow field opposing the shaft rotation significantly intensified these secondary recirculation zones and thus reduced the average circumferential velocity: injection or preswirl in the direction of rotation significantly weakened these zones. A decrease in average circumferential velocity was related to an increase in the strength of the recirculation zones and thereby promoted stability. The influence of the axial flow was analyzed. The lumped model of fluid dynamic force based on the average circumferential velocity ratio (as opposed to the bearing/seal coefficient model) well described the results obtained for relatively large but limited ranges of parameters. This lumped model is extremely useful in rotor bearing/seal system dynamic analysis and should be widely recommended. Fluid dynamic forces and leakage rates were calculated and compared with seal data where the working fluid was bromotrifluoromethane ($CBrF_3$). The radial and tangential force predictions were in reasonable agreement with selected experimental data. Nonsynchronous perturbation provided meaningful information for system lumped-parameter identification from numerical experiment data.

INTRODUCTION

Much of the current research on seal- or bearing-driven instabilities in turbomachines is contained in NASA publications (refs. 1 to 5). Topics such as seal dynamic coefficients (as measured by Childs, Benckert, Wyssman, Iwatsubo, and others), analytical methods (Fleming, Nelson, Black, Brown, Muszynska, Bently, and others), numerical techniques (Tam, Przekwas, Rhode, Nordmann, and others), and practical applications (gas injection and swirl brakes) are but a sampling of the research efforts of the past decade. For example, in the mid-1970's seals were identified as contributors to turbomachine instabilities. In 1977, fluid nitrogen and hydrogen data for straight and three-step cylindrical space shuttle main engine (SSME) seal configurations were available over a wide range of thermodynamic states for concentric and eccentric seals but without rotation. By 1978, four basic seal configurations were targeted for investigation: bore (cylindrical), face, labyrinth, and tip; honeycomb was added later. It was thought that with a fundamental understanding of these configurations, any type of seal (bearing) could be designed for stable operations. By 1980, techniques were developed to cope with units that proved to be unstable, but the degree of understanding was inadequate to design stable high-performance turbomachinery. Further, the stability of a new or upgraded design could only be demonstrated by full-load operation in place (ref. 1). By 1982, several programs had been put into place that began to systematically resolve problems of predicting stability characteristics and experimental validation of forces that influence rotordynamics (ref. 2). By 1984, test results were presented and new data to be used in designing turbomachinery were available. But, as in all research fields, with understanding comes realization of one's ignorance.

Many discrepancies now began to appear, and despite some progress, the problem of predicting and adequately modeling fluid dynamic forces applied to rotors and predicting instabilities does not seem to be in danger of imminent extinction (ref. 3). Now more often the end user and manufacturers joined the effort rather than pursuing the usual quick-fix and shotgun approach. Problems were being cured directly in the field (ref. 5). By 1986, manufacturers were presenting results related to experience, philosophy of design, and on-line operations of compressors. Computational fluid dynamics (CFD) was introduced in an attempt to merge the classical dynamics approach with that of the actual flow field. Swirl brakes and antiswirl methodology, although not entirely understood, were being applied with significant success (refs. 4 to 11). Data providing dynamic coefficients for turbomachine design were forthcoming from several foreign and domestic sources (refs. 5 and 12). Of particular significance are the data of Braun et al. (ref. 13), which quantified the flow fields near the minimum clearance for both the convergent and divergent zones of a simulated bearing.

The existing fluid-force lumped model based on bearing/seal coefficients, although mathematically simple, revealed the lack of understanding of the physical phenomena taking place in bearings and seals and proved to be insufficient to describe these forces adequately. An advanced model based on fluid average circumferential velocity ratio is used in this paper.

Though this review is brief, perhaps terse, one becomes aware that although the primary function of a seal is to control leakage, a secondary but equally important purpose is to provide (or at least not to infringe on) rotordynamic stability. Bearings also have a dual role, namely to support the rotor

load and provide dynamic stability. Seal and bearing combinations can be used to enhance stability as well as to decrease bearing loads. Further, the flow fields in bearings and seals possess similarities although with some distinct differences. The axial pressure drop in the seal is large and the circumferential pressure drop is nominally smaller. For the bearing the opposite holds true. Further, zones of secondary flow appear inevitable. Cavitation phenomena can occur in both bearings and seals in the form of either gaseous cavitation (pressure lower than atmospheric) or vaporous cavitation (pressure lower than saturation pressure). The latter can be related to thermodynamic phase changes due to changes in pressure and velocity at inception zones of secondary flows. It is apparent that local bulk flow models are inadequate even though they may serendipitously predict system dynamics and have been successfully used by many authors. It is to this false sense of security that this paper is addressed. It is concluded that a seal or bearing properly designed by using computational fluid dynamics and knowledge-based methodologies can enhance turbomachine stability.

SYMBOLS

A	amplitude of rotor precession
b,α	coefficients in the Prandtl mixing-length model
c	bearing (or seal) radial clearance
D	fluid radial damping
dv	transformed space volume element ($\equiv 1$)
$d\xi^{1,2,3}$	transformed space arc lengths in three coordinate directions
$\vec{e}(\vec{e}_1,\vec{e}_2,\vec{e}_3)$	unit vector
F_r,F_t	fluid dynamic radial and tangential forces, respectively
$\vec{g}$	gravity vector
$h_{1,2,3}$	scale factors in three coordinate directions
J	determinant of Jacobian matrix
$j = \sqrt{-1}$	
K	fluid radial stiffness coefficient
K_{xy}	fluid tangential stiffness coefficient (cross-coupled stiffness)
$k-\varepsilon$	turbulence energy production-dissipation
ℓ	seal or bearing length
ℓ_m	mixing length scale of seal

M	fluid inertia
P_{in}, P_{out}	inlet and outlet axial pressures
p	fluid pressure
R	seal or bearing radius
R_i	shaft radius
r	fluid local radius in bearing/seal clearance
$\vec{r}$	displacement vector
t	time
$\vec{U}$	fluid velocity vector
$\vec{\tilde{U}}$	reference frame velocity vector
$\tilde{u}, \tilde{v}$	reference frame circumferential and radial velocity components, respectively
Vol_{cell}	physical volume of a grid cell
Z	axial coordinate in bearing or seal
$z = x + jy$	shaft radial displacement
z_r	radial displacement magnitude of z
$\Delta P = P_{in} - P_{out}$	axial pressure drop
$\vec{\varepsilon}$	contravariant base vector
ζ	normal distance between housing and shaft surfaces
κ_D	fluid direct dynamic stiffness
κ_Q	fluid quadrature dynamic stiffness
λ	fluid average circumferential velocity ratio
λ_e	preswirl-related fluid average circumferential velocity ratio
λ_i	injection-related fluid average circumferential velocity ratio
μ_t	turbulent viscosity
ν	fluid kinematic viscosity
ρ	fluid density

τ	stress tensor
Φ	angular coordinate in bearing or seal
ϕ	rate of strain in Newtonian fluid
ω_p	rotor precession (perturbation) frequency, or angular velocity
ω_R	rotative speed
∇	gradient

Superscripts:

$\rightarrow$	denotes vector
$\approx$	denotes tensor

NUMERICAL APPROACH

Consider a shaft rotating clockwise at rotative speed ω_R and precessing with amplitude A (dynamic eccentricity) at rotor precession (perturbation) frequency ω_p within a static cylindrical housing (fig. 1). The housing configuration can represent a seal or a bearing. With the presence of axial pressure drop significant Coriolis forces are generated. Additionally, centrifugal forces at the inlet as well as convergent/divergent zones occur. These forces are major contributors to dynamics, as illustrated below by numerical solutions.

The problem here is that we are dealing with nonconventional flow fields in very narrow passages and the passage geometry is changing periodically with time. In order to adequately simulate seal or bearing flows, the fluid motion is best described by a three-dimensional rotating coordinate frame attached to the rotor and precessing with it at perturbation frequency ω_p. In this coordinate system the given bearing/seal geometry is invariant in time (refs. 14 to 16) since the precession motion of the rotor center with respect to the housing centered position (zero static eccentricity) is assumed to be restricted to a circular orbit. It should be mentioned here that more complex assumptions concerning the rotor orbit (e.g., elliptic, nonzero static eccentricity) will let the flow domain become time dependent, and analysis with time-variable functions should be performed accordingly.

In general, for an observer located in the rotating frame the relation between absolute, relative, and grid velocity becomes

$$\vec{U}_{abs} = \vec{\tilde{U}} + \vec{\omega}_p \times \vec{r} \tag{1}$$

where $\vec{U}_{abs}$ is the fluid absolute velocity, $\tilde{U}$ is the fluid relative velocity, $\vec{\omega}_p$ is the rotor precession (perturbation) frequency, and $\vec{r}$ is the local radius in the fluid.

Governing Equations

The subsequent equation for the conservation of mass can be written as

$$\frac{\partial}{\partial t}(\rho J) + \nabla \cdot (\rho \vec{\tilde{U}}) J = 0 \tag{2}$$

where ρ is the fluid density and J is the determinant of the Jacobian matrix (i.e., the physical volume of a grid cell in the finite difference approach).

The Jacobian matrix is calculated for each of the control volumes as

$$J = (\vec{\varepsilon}_1 \times \vec{\varepsilon}_2) \cdot \vec{\varepsilon}_3 = h_1 h_2 h_3 [(\vec{e}_1 \times \vec{e}_2) \cdot \vec{e}_3]$$

where $\vec{\varepsilon}$ and $\vec{e}$ are the contravariant base and unit vectors, respectively, and h_1, h_2, and h_3 are the scale factors in three coordinate directions. The correlation between the Jacobian matrix and the physical cell volume comes from the definition of the volume element:

$$dV = \vec{\varepsilon}_1 \cdot (\vec{\varepsilon}_2 \times \vec{\varepsilon}_3) d\xi^1 \, d\xi^2 \, d\xi^3 = J \, d\xi^1 \, d\xi^2 \, d\xi^3 = J \, dv$$

where dV is the physical volume element, dv is the transformed space volume element, and $d\xi^1$, $d\xi^2$, and $d\xi^3$ are the transformed space arc lengths along three coordinate directions.

By using the Euler identity and assuming a small circular orbit of the rotor precessing about the housing center, the rate change of the Jacobian matrix can be made to vanish. As a consequence, the "quasi-steady" analysis is valid and equation (2) takes the final form

$$\nabla \cdot (\rho \vec{\tilde{U}}) J = 0 \tag{3}$$

The three-dimensional turbulent time-averaged "conservative"[1] Navier-Stokes (N-S) equation in the coordinate system rotating at the perturbation angular velocity ω_p is

$$\frac{\partial(\rho \vec{\tilde{U}} J)}{\partial t} + \nabla \cdot (\rho J \vec{\tilde{U}} \vec{\tilde{U}}) = -J \nabla p - J[\underbrace{\rho \vec{\omega}_p \times}_{\text{Centrifugal}} (\vec{\omega}_p \times \vec{r}) + \underbrace{2\rho \vec{\omega}_p \times \vec{\tilde{U}}}_{\text{Coriolis}}] + \underbrace{J \nabla \cdot \tilde{\tilde{\tau}}}_{\text{Shear}} + \underbrace{J \rho \vec{g}}_{\text{Body force}} \tag{4}$$

It is very important to note the centrifugal and Coriolis source terms arising from the shaft whirling at ω_p.

In this equation the term $\nabla \cdot \tilde{\tilde{\tau}}$ represents combined normal and shear stress components. In the present analysis a Newtonian fluid is assumed with a stress tensor proportional to the rate of strain: $\tau_{ij} = 2\mu\phi_{ij}$. The centrifugal and Coriolis forces appear to be caused by the coordinate rotation and are

---

[1] Conservation is respected at every grid point in the mesh; viscous fluctuating terms are time averaged.

incorporated into the computational model as additional volumetric momentum sources.

When the N-S equation is expressed in terms of velocity component equations (in the rotating frame), the extra source terms (Coriolis and centrifugal) for $\tilde{u}$ and $\tilde{v}$ momentum equations (circumferential and radial) arise:

$$S(\tilde{u}) = -2\rho\omega_p\tilde{v}\ Vol_{cell}, \qquad S(\tilde{v}) = (\rho\omega_p^2 r + 2\rho\omega_p\tilde{u})\ Vol_{cell} \tag{5}$$

where Vol_{cell} is the physical volume of a grid cell (from J).

Choice of Turbulence Model

A brief review of turbulence models is given in the appendix. Because fluctuation details for high shear flows at low clearances are not yet available, the simplest of the turbulence models was selected for the present calculations.

The characteristics of seal and bearing flows can be summarized as strong swirl, high viscosity, and high pressure drop associated with significant wall roughness and small clearances. As a consequence, it is more appropriate to use a simple approach such as the zero-equation Prandtl mixing length model. This model takes into consideration the above-mentioned factors and it has undoubted advantages, such as (a) that it is simple and well established and (b) that the mixing length scale is determined by the clearance. The resulting Navier-Stokes equations describe the time-averaged distributions of velocity and pressure, etc. It is noted that the stress tensor introduced earlier now also contains Reynolds stress terms involving $-\rho\overline{u_i' u_j'}$. The turbulence model currently used in the seal/bearing flow simulation makes use of the eddy-viscosity concept to compute the Reynolds stresses ($\mu_t = \rho\ell_m^2\phi$, where μ_t is the turbulent viscosity, ℓ_m is the mixing length, and ϕ denotes the rate of strain).

The mixing length ℓ_m is characterized as (ref. 17)

$$y/\zeta \le \alpha/b, \quad \ell_m/\zeta = by/\zeta, \quad b = 0.435, \quad y/\zeta > \alpha/b, \quad \ell_m/\zeta = \alpha, \quad \alpha = 0.09$$

where ζ is the normal distance measured between the stator and the rotor surfaces; y is the minimum local distance measured from the stator and rotor surfaces; and b and α are coefficients.

Solution Method

In the employed numerical method the governing transport equations are solved simultaneously by a fully conservative, finite difference (or control volume) approach using the SIMPLEST algorithm (ref. 18). SIMPLEST solves the continuity equation by using a fast "whole field" solver and solves the velocity components by using Jacobi's point-by-point algorithm. A Newton-Raphson method is used to express the convective fluxes in the continuity equation in terms of pressure correction. Salient features of the employed method are the

use of an upwind differencing scheme and a staggered-grid practice for the convective flux calculation, as well as the integrated sources in the Newton-Raphson linearized form. These practices are used to enhance numerical stability.

Boundary Conditions

The boundary conditions for seal/bearing flow calculations include specified pressure at the flow inlet and outlet; circumferential velocity at the inlet (without or with preswirl); rotor rotative speed and rotor precessional speed; no-slip velocity condition at the rotor and stator walls; fluid shear stresses on the surfaces of the rotor and stator; and cyclic boundary conditions in the circumferential direction. Shear stresses on the rotor and stator surfaces are calculated on the basis of the Couette flow assumption. The universal "log-law" of the wall function approach is adopted. The experiments set up by Childs et al. (refs. 1 to 4) indicate that the surface roughness treatment depends on the flow direction (i.e., there is higher resistance to flow in the axial than in the circumferential direction). Consequently different rough-to-smooth correlations are specified in the axial and circumferential directions (the coefficients 2.9 and 1.1 were used as multipliers in the smooth friction relations correspondingly). These factors were determined by trial calculations of a base case to obtain axial pressure variations similar to that of the corresponding experiments.

Computational Grid

A three-dimensional, nonorthogonal, body-fitted computational grid up to NX × NY × NZ = 12 × 6 × 16 = 1152 control volumes has been selected for the computations (fig. 2). The grid allows for steep variations in physical parameters (fluid preswirl in particular).

Fluid Dynamic Force

The three-dimensional, flow-related local fluid dynamic forces are integrally averaged over the entire configuration. It is supposed that the integral averaging procedure yields one equivalent lumped fluid dynamic force represented by three components: radial, tangential, and axial.

Fluid circumferential force components F_r (radial) and F_t (tangential) are calculated from the pressure distribution:

$$-F_r = \int_0^{2\pi}\int_0^{\ell} p\cos(\phi)R_i\, d\phi dZ \qquad -F_t = \int_0^{2\pi}\int_0^{\ell} p\sin(\phi)R_i\, d\phi dZ \tag{6}$$

where R_i is the shaft radius, ℓ denotes bearing or seal length, and ϕ is the angle measured (clockwise) from the position of minimum clearance.

The third component of the fluid force F_z is related to the axial flow such as that occurring in seals of pumps and compressors due to balance piston loading. In bearings F_z is usually small relative to F_r and F_t, but for seals in machines of SSME category the axial flow is large and F_z has a significant value. F_z reflects the axial thrust and local changes in momentum

and can be represented as the product of the axial pressure drop Δp and the clearance area $\pi(R^2 - R_i^2)$. However, F_z remains implicitly linked to F_r F_t.

With the assumption of constant precession (perturbation) amplitude the radial and tangential force component amplitudes in the rotating coordinates have the same form as in the stationary coordinate system.

NUMERICAL RESULTS

Three-dimensional-flow numerical results show significant changes in the local values of the fluid dynamic force along the seal (or bearing). They also show the existence of significant secondary flows and local separations even in case of a large axial pressure drop.

Most of the results of flow calculations pertinent to the rotor stability (mainly the circumferential flow) are presented in the integrally averaged form of fluid direct κ_D and quadrature κ_Q dynamic stiffnesses yielded by fluid radial F_r and tangential F_t force components divided by precession amplitude A. The dynamic stiffnesses are plotted versus perturbation frequency ω_p (or its modified forms which, for specific cases, are defined below). The fluid-force components in the dynamic stiffness format are easily comparable to experimental results for synchronous ($\omega_p = \omega_R$) (refs. 2 and 19) as well as nonsynchronous ($\omega_p \neq \omega_R$) perturbation (ref. 20). The nonsynchronous perturbation yields the best identifiable results for building fluid-force lumped models. In the present study only <u>forward</u> perturbation was used (ω_p and ω_R in the same direction).

Input Parameters

The input parameters for the calculated examples are give in tables 1 and 3. Table 1 also contains the calculated total average leakage and axial force for each case. The rest of the results are illustrated in figures 3 to 17. Although the input data cases were quite limited, the numerical results brought a wide spectrum of fluid dynamic phenomena that will certainly require further investigation. Calculating cases with intermediate values of the input parameters and consistently using forward as well as backward nonsynchronous perturbation (not to limit studies to synchronous perturbation) seems an important necessity before generalizations for lumped models can be completed.

Comparison With Experimental Data

Numerical results are compared in figure 3 with experimental results obtained by Childs (refs. 2 and 19). Although there were three steps within the length of the experimental seal the modeled seal was for simplicity considered as a straight cylindrical seal without inlet preswirl, the experiment and the calculations qualitatively agreed. The calculated direct dynamic stiffness decreased with speed but did not exhibit the negative values of the experimental data at elevated rotor speed. The omission of the internal steps may account for this discrepancy. The quadrature dynamic stiffness increased

with rotative speed and agreed reasonably well with the data of Childs (ref. 2).

Lumped-Parameter Model of Fluid Circumferential Force

For certain cases the fluid circumferential force components are easily identifiable in the lumped form model when the notion of fluid average circumferential velocity ratio[2] λ (refs. 21 and 22) is taken into consideration as a key parameter in this model.

The model with fluid average circumferential velocity ratio proved to be much more powerful and described the physical meaning of the fluid force more accurately than traditional bearing/seal coefficient modeling (refs. 20 to 22). This model is directly adopted from the cases in which the axial flow is uncoupled from the circumferential flow. It is supposed that the axial flow affects the circumferential flow in a parametric way only (refs. 21 to 25). The importance of the model lies in its direct correlation to rotation-related circumferential flow parameters, as they represent major factors in rotor stability.

The lumped model of the fluid circumferential force is based on the assumption that because of shaft-rotation-related fluid involvement in circumferential motion, the fluid dynamic force is rotating at the angular speed $\lambda\omega_R$ (not a constant $\omega_R/2$, as is often assumed (refs. 23 to 25)). In the coordinate system rotating at angular speed $\lambda\omega_R$ the fluid dynamic force has three radial components: stiffness force (proportional to shaft radial displacement z_r), damping force (proportional to shaft radial velocity $\dot{z}_r$), and fluid inertia (proportional to radial acceleration $\ddot{z}_r$) (refs. 21 to 26), where z is complex. For clarity the additional tangential as well as nonlinear components are omitted in this presentation. Transformation of the fluid rotating force to the stationary inertial coordinates introduces complex expressions for acceleration and velocity. The fluid force becomes

$$-F = Kz + D(\dot{z} - j\lambda\omega_R z) + M(\ddot{z} - 2j\lambda\omega_R\dot{z} - \lambda^2\omega_R^2 z)$$

$$z = x + jy, \qquad j = \sqrt{-1}, \qquad |z| = \sqrt{x^2 + y^2}, \qquad \cdot = d/dt \tag{7}$$

where K, D, and M are fluid radial stiffness, damping, and inertia coefficients correspondingly and z is shaft radial displacement (conventionally, x denotes horizontal, y denotes vertical), and $z = z_r e^{j\lambda\omega_R t}$ is the transformation from stationary to rotating coordinates. In the bearing/seal

---

[2]The fluid velocity is inferred from the force calculations that represent the interaction of local fluid forces integrally averaged over the entire configuration. Local variations in forces and velocity are strong, but for modeling purposes single averaged values are assumed for the force and the flow velocity. Fluid average circumferential velocity ratio λ can be identified as the ratio between whirling and rotative speeds ("whirl" = rotor self-excited lateral vibrations (ref. 22)).

coefficient format and in the chosen reference system (fig. 1) the fluid force for clockwise rotation is as follows:

$$-F = \frac{1}{|z|}\begin{vmatrix} -F_r & -F_t \\ F_t & -F_r \end{vmatrix}\begin{vmatrix} x \\ y \end{vmatrix} = \begin{vmatrix} K - M\lambda^2\omega_R^2 & D\lambda\omega_R \\ -D\lambda\omega_R & K - M\lambda^2\omega_R^2 \end{vmatrix}\begin{vmatrix} x \\ y \end{vmatrix}$$

$$+ \begin{vmatrix} D & 2M\lambda\omega_R \\ -2M\lambda\omega_R & D \end{vmatrix}\begin{vmatrix} \dot{x} \\ \dot{y} \end{vmatrix} + \begin{vmatrix} M & 0 \\ 0 & M \end{vmatrix}\begin{vmatrix} \ddot{x} \\ \ddot{y} \end{vmatrix} \tag{8}$$

Note that the "cross-coupled stiffness" term is generated here by the radial damping due to rotation and is proportional to λ and ω_R. The radial stiffness is modified by centrifugal inertia and carries the negative sign. "Cross damping" is due to the Coriolis inertia force. The model can easily be extended and completed with other terms such as additional tangential stiffness K_{xy} (modifying $D\lambda\omega_R$ into $D\lambda\omega_R + K_{xy}$).

When the shaft precessional motion is circular with frequency ω_p and amplitude A, that is,

$$z = Ae^{j\omega_p t} \tag{9}$$

and (eq. (9)) is substituted into (eq. (7)), the fluid force becomes

$$-F = A[K + jD(\omega_p - \lambda\omega_R) - M(\omega_p - \lambda\omega_R)^2]e^{j\omega_p t}$$

The force amplitude divided by the motion amplitude A yields the complex dynamic stiffness κ:

$$\left|\frac{-F}{A}\right| = \kappa = \kappa_D + j\kappa_Q \equiv K - M(\omega_p - \lambda\omega_R)^2 + jD(\omega_p - \lambda\omega_R) \tag{10}$$

with direct (real) κ_D and quadrature (imaginary) κ_Q components.

Results of Nonsynchronous Forward Perturbation

The results of calculations for nonsynchronous perturbation cases are shown in figures 4 to 7. The ratio of tangential force to precession amplitude (with opposite sign), representing fluid quadrature dynamic stiffness κ_Q, is plotted versus perturbation frequency ω_p (fig. 4). From this numerical experiment the result is a straight line that allows one to identify the fluid radial damping D and the average circumferential velocity ratio λ for the lumped model (eq. (8)) (refs. 21 and 22).

$$\kappa_Q = D(\omega_p - \lambda\omega_R) \tag{11}$$

The identified ratio λ can then be used to modify the abscissa for the direct dynamic stiffness results (fig. 5). Instead of ω_p the expression $(\omega_p - \lambda\omega_R)^2$ for each corresponding rotative speed ω_R has been used. The ratio of radial force to precession amplitude (with opposite sign) has been identified as

$$\kappa_D = K - M(\omega_p - \lambda\omega_R)^2 \tag{12}$$

where K and M are the fluid radial stiffness and inertia, respectively. The direct dynamic stiffness versus modified perturbation frequency is again a straight line allowing for easy identification of the parameters (fig. 5).

The form of the fluid dynamic force model (eq. (7)) has been identified through experimental nonsynchronous perturbation testing (ref. 20). A quantitative comparison of experimental and numerical results has not been done, since such a numerical case, which should include rotor parameters, has not yet been calculated. Qualitatively, however, the numerical results for considered cases reflect good adequacy of the lumped model (eq. (7)), which emphasizes the role of rotation-generated circumferential flow. Note the high value of the fluid inertia, $M = 4.63$ kg (fig. 5). It exceeds about 400 times the fluid mass in the seal (data from tables 2 and 3). The relatively low value of λ identified from the numerical experiment may be due to lack of rotor dynamic parameters in the model.

Nonlinear Considerations

Nonlinearity of the fluid dynamic force should be taken into consideration in more advanced lumped models. K and D as well as λ are nonlinear functions of shaft eccentricity. Figure 6 illustrates the effect of nonlinearity. For $A = 0.5c$ (where c is bearing or seal radial clearance) the dynamic stiffnesses are higher than for $A = 0.24c$. Their shapes, however, are very close (except for low rotative speed). When the same fluid force models (eqs. (7) and (8)) are used as previously, the results mean that the fluid radial stiffness K is a nonlinear increasing function of shaft eccentricity (the most pronounced effect) and that fluid average circumferential velocity ratio λ is a decreasing function of eccentricity (lesser effect). The effect of eccentricity on the fluid radial damping D and the fluid inertia in the considered range of parameters is not very high.

Seal Secondary Flow

Figure 7 presents the influence of rotation and perturbation speeds on the secondary flow patterns in seal flows. Lower rotative speed and higher perturbation speed intensified the secondary flow zones and by lowering the average circumferential velocity enhanced rotor stability. For the assumed geometry and the considered range of pressure drop (17 bars) the secondary flow zone occurred just in front of the minimum clearance or convergence zone. Note that this zone rotates with frequency ω_p.

Preswirl and Pressure Drop Effects

Figures 8 and 9 show results of calculations for the seal flow with preswirl for two values of the axial pressure drop. The preswirl was imposed at the seal inlet in either the forward or backward circumferential direction in the following form:

$$V_{ps} = R_i \omega_R \, [1 - r/R]^{1/3} \tag{13}$$

where V_{ps} is the preswirl circumferential velocity at radius r; R_i and R are shaft and seal radii correspondingly. The preswirl clearly modifies the fluid average circumferential velocity ratio λ and is introduced to the model previously discussed in the form of an average value λ_e which is negative for the preswirl against the direction of rotation (resultant λ is lower) and positive for the preswirl in the direction of rotation. In the latter case the circumferential mass flow and fluid velocity are clearly intensified and λ increases.

In this numerical case the perturbation was synchronous ($\omega_p = \omega_R$); therefore full identification of the model parameters was not possible (figs. 8 and 9).

For higher axial pressure drop the fluid force components exhibited linear relationships with perturbation frequency and perturbation frequency squared correspondingly (again for direct dynamic stiffness the perturbation frequency was modified by using the same algorithm as in the previous case, illustrated in figure 5, now with $\omega_p = \omega_R$ taken into account, fig. 8). For lower pressure drop the fluid force components exhibited higher λ (circumferential flow intensified), lower D, K, and M, and more nonlinear character versus ω_R^2 and ω_R correspondingly (figs. 8 and 9). High pressure drop means that there is a significant axial flow in the seal. Higher values of fluid radial stiffness, damping, and inertia in this case are intuitively easily understood (if one neglects the secondary flows). The lower average circumferential velocity ratio for higher axial pressure drop also fits well with the physical interpretation of the phenomenon: The axial flow is dominant and the circumferential flow is reduced (fig. 10).

When the data were extrapolated (fig. 9), a slight discrepancy between ratios of λ_e to $(1 - \lambda)$ was identified from direct and quadrature dynamic stiffnesses, and the additional cross-coupled term K_{xy} (tangential component in the model of the form $-jK_{xy}z$ when added to eq. (7)) appeared. This will require further investigations, using in particular the nonsynchronous perturbation.

Figure 11 illustrates the influence of the inlet preswirl on the secondary (backward) circumferential flow field. It is evident that the preswirl intensifies the recirculation zone if it is introduced in the direction opposite to rotation (lower resultant λ, higher rotor stability). Preswirl in the direction of rotation weakens the recirculation zone and intensifies forward circumferential flow (higher resultant λ).

Fluid Injection Effects

Figures 12 to 14 illustrate the influence of fluid injection on dynamic stiffnesses. Three cases with injection were considered: radial, in the direc-direction of rotation, and against rotation. Figure 12 gives the corresponding angular relations. Injection rate was proportional to rotative speed (table 1).

In comparison to the case with no injection, the resultant dynamic stiffnesses were considerably modified. All parameters exhibited nonlinear character, as functions of rotative speed. Fluid radial stiffness increased and fluid inertia decreased. Following the previously discussed model, the fluid effective damping $D(1 - \lambda + \lambda_i)$ increased when injection was against rotation ($\lambda_i < 0$, where λ_i is the injection-related average circumferential velocity ratio) and decreased when injection was in the direction of rotation ($\lambda_i > 0$). The radial injection caused a higher radial stiffness K and a lower λ than in the no-injection case, which is a very important observation for pressurized, fluid-lubricated bearings as well as for "anti-swirl" seal techniques.

Here again, the application of synchronous perturbation only (as opposed to nonsynchronous) did not allow for the full identification of the parameters.

Average Leakage

Results of the leakage calculation are presented in table 1. The effect of rotation and perturbation speed on the leakage value was most pronounced when the axial pressure drop was assumed low. Increasing rotative speed reduced leakage (more fluid involved in circumferential motion). Increasing perturbation speed increased leakage (pumping effect). In cases with fluid injection the highest leakage occurred when injection was in the direction of rotation. Injection against rotation reduced the leakage by about 7 percent.

Circumferential Force Versus Axial Force

In all calculated cases the pressure drop was relatively low. The resulting axial forces did not exceed 300 N (table 1). For the assumed precessional amplitudes the maximum circumferential forces were usually much higher, especially their tangential components ($F_{t,max} \approx 750$ N in case 2, $F_{t,max} \approx 600$ N in case 4b, $F_{t,max} \approx 800$ N in case 5). Maximum radial force was usually about 50 percent smaller than the maximum tangential force.

BEARING FLOWS

Bearing flows were numerically simulated by assuming higher fluid viscosity and low axial pressure drops (tables 1 to 3).

Bearing Secondary Flow

Figure 15 illustrates the influence of rotation and perturbation speed on the secondary flow patterns in bearing flows. For this case the axial pressure drop was low ($\Delta p = 0.3$ bars). Compared to figure 7, where axial pressure drop

lack of rotordynamic parameters in the model. By maintaining the clear physical interpretation this model represents a significant refinement of the bearing/seal coefficients. Furthermore, since the lumped parametric forms also agree with experimental results, the model can be adjusted so that the numerical experiments and the physical experiments agree. The nonsynchronous perturbation proved to be very efficient in identifying lumped model parameters from numerical and experimental (ref. 20) data.

The numerical experiments delineated regions of secondary flows. These zones were intensified with preswirl opposing shaft rotation. In terms of the proposed lumped model the integrally averaged fluid circumferential velocity ratio decreased; this implied a stabilizing influence for rotors. Numerical experiments with fluid injection indicate a similar response, which is of significance not only to pressurized fluid-lubricated bearing designs, but to "antiswirl" controls as well. Furthermore, calculated primary and secondary circumferential flows in a simulated bearing were found to be in good agreement with physical experiments.

For further studies the current version of the computer code should be expanded to include the energy equation, rotor static eccentricity, and elliptic perturbation orbits, as well as rotor mechanical parameters. Although these additions will require time-dependent solutions of the transformed Navier-Stokes equations (i.e., much more complex numerical algorithms), the results would begin to properly simulate reality.

was higher (more like that taking place in seals), the secondary flows occurred at a high clearance region and were less intense than in the "seal" case.

Axial Versus Circumferential Flow

Figures 16 and 17 present the relationships between the circumferential and axial nonwhirling flows in an oil bearing with large clearance (table 3). To model the oil bearing case, ω_p was set to zero; A became the static eccentricity; the source terms $S(\tilde{u})$ and $S(\tilde{v})$, equation (5), were zero and the governing equations (4) reverted to unmodified cylindrical form. The figures illustrate axial flow velocity and circumferential flow patterns frozen at the shaft's lowest vertical position and at several axial locations. The axial pressure drop proved to be a very important factor in reducing the secondary flows. For case 7 (fig. 16) the pressure drop was zero. At the smallest clearance the axial flow velocity was consistently zero, but the oil was axially pumped out of and into the bearing in the convergent and divergent zones, respectively. The secondary flow zones existed in the high clearance area along the entire axial length of the bearing. During flow visualization experiments (Braun, et al.) such "stagnation" zones were clearly observed (ref. 13).

The existence of a tiny axial pressure drop (Δp = 0.1 bar, fig. 17) significantly changed the flow pattern. Secondary flows were much smaller and appeared just before the narrowest clearance and only on the bearing inlet side. The axial flow was not uniform through the bearing. Regions of axial flow reversal (negative velocity) developed just in front of the narrowest clearance. Note that in figures 16 and 17 the shaft was actually rotating at the frequency (with $\omega_p = 0$) and in both considered cases the ratio of bearing clearance to shaft radius was very high. The flow pattern for more realistic bearing parameters may look significantly different. The preliminary calculations do illustrate the persistence of secondary flows in bearings with conventional clearance-to-radius ratios. These flows exhibit, however, lower intensity than for bearings with large clearances and without perturbation velocity ω_p. Furthermore, extremely fine grids should be used in order to delineate flow field details.

CLOSING REMARKS

Significant progress in computer technology now allows for high-speed, highly accurate calculations of three-dimensional fluid flows at relatively low costs. This paper advances a numerical model based on the transformed three-dimensional, turbulent, conservative Navier-Stokes equations that is applicable to seals and bearings. Leakages and fluid dynamic forces were calculated and found in good agreement with selected data of Childs (refs. 2 and 19). Several numerical experiments were performed and related to a lumped-parameter model that a priori assumes the existence of an integrally averaged circumferential velocity representative of the configuration flow field. Rotor stability is directly correlated with circumferential flow (ref. 26). The fluid average velocity ratio is an effective measure of the circumferential flow and thus represents a meaningful parameter for rotordynamics. To the first order, lumped parameters were extracted from the numerical experiments. Relatively low values of the circumferential velocity ratio can be associated with the

$$\rho \frac{D\varepsilon}{Dt} = \frac{\partial}{\partial x_i}\left(\frac{\mu_t}{\sigma_\varepsilon}\frac{\partial \varepsilon}{\partial x_i}\right) + \frac{\varepsilon}{k}\left[C_1 \mu_t \left(\frac{\partial u_i}{\partial x_j} + \frac{\partial u_j}{\partial x_i}\right)\frac{\partial u_j}{\partial x_i} - C_2 \rho \varepsilon\right]$$

Total derivative of turbulence dissipation — Diffusion — Production — Dissipation

$$\mu_{eff} = \mu + \frac{C_\mu \rho k^2}{\varepsilon}$$

Effective viscosity — Molecular viscosity — Turbulent viscosity

(iv) Multiequation of Reynolds-stresses model (e.g., tranport equations for the turbulent stresses containing triple correlation of fluctuating velocities provided for $\overline{u_i' u_j'}$, $\overline{u_i'^2}$, $\overline{u_i' u_j'^2}$, and ε):

$$\frac{D\overline{u_i' u_j'}}{Dt} = P_{ij} + \pi_{ij} + D_{ij} - \varepsilon_{ij}$$

Total derivative of individual Reynolds stress — Generation tensor — Pressure strain (redistribution) — Diffusion — Viscous dissipation

$$\mu_{eff} = \mu + C_\mu \rho \sqrt{k}\ell$$

Effective viscosity — Molecular viscosity — Turbulent viscosity

There is a considerable amount of evidence that one-, two-, or multiequation models of turbulence are still not satisfactory for flows that exhibit strong swirl, curvature, highly viscous, and low-Reynolds-number effects (ref. 17). Some researchers claim, however, successful application of the k-ε model to seal flows (e.g., ref. 10).

APPENDIX - TURBULENCE MODELS

A fluid motion is described as turbulent if it is rotational, intermittent, highly disordered, diffusive, and dissipative. The turbulence quantities based on the Reynolds equation and the Reynolds stress term can be modeled by using the second-order closure form of their balance equations and generally can be expressed in terms of time-averaged variables. There are several turbulence models that can be used to simulate the turbulent flow using Navier-Stokes equations (for comprehensive review see ref. 17).

The main classes of turbulence models are as follows:

(i) Zero-equation (e.g., Prandtl mixing length model):

$$\mu_{eff} = \mu + \rho \ell_m^2 \phi$$

Effective viscosity	Molecular viscosity	Turbulent viscosity

(ii) One-equation model of turbulence (e.g., turbulence kinetic energy k):

$$\rho \frac{Dk}{Dt} = -\frac{\partial}{\partial x_i}\left(\rho \overline{u_i' k'} + \overline{p' u_i'}\right) - \rho \overline{u_i' u_j'}\left(\frac{\partial \bar{u}_i}{\partial x_j}\right) - \mu \sum_{ij} \overline{\left(\frac{\partial u_j'}{\partial x_i}\right)^2}$$

Total derivative of turbulence kinetic energy	Diffusion	Production	Dissipation

$$\mu_{eff} = \mu + C_\mu \rho \sqrt{k} \ell$$

Effective viscosity	Molecular viscosity	Turbulent viscosity

(iii) Two-equation model of turbulence (e.g., k-ε model):

$$\rho \frac{Dk}{Dt} = \frac{\partial}{\partial x_i}\left(\frac{\mu_t}{\sigma_k}\frac{\partial k}{\partial x_i}\right) + \mu_t \left(\frac{\partial u_i}{\partial x_j} + \frac{\partial u_j}{\partial x_i}\right)\frac{\partial u_j}{\partial x_i} - \rho\varepsilon$$

Total derivative of turbulence kinetic energy	Diffusion	Production	Dissipation

REFERENCES

1. Childs, D.W., Vance, J.M., Hendricks, R.C., eds., Rotordynamic Instability Problems in High-Performance Turbomachinery - 1980, NASA CP-2133, 1980.

2. Childs, D.W., Vance, J.M., Hendricks, R.C., eds., Rotordynamic Instability Problems in High-Performance Turbomachinery - 1984, NASA CP-2338, 1984.

3. Childs, D.W., Vance, J.M., Hendricks, R.C., eds., Rotordynamic Instability Problems in High-Performance Turbomachinery - 1982, NASA CP-2250, 1982.

4. Childs, D.W., Vance, J.M., Hendricks, R.C., eds., Rotordynamic Instability Problems in High-Performance Turbomachinery - 1986, NASA CP-2443, 1986.

5. Bently, D.E., Muszynska, A., Hendricks, R.C., eds., Instability in Rotating Machinery, NASA CP-2409, 1986.

6. Ambrosch, F., and Schwaebel, R., "Method of and Device for Avoiding Rotor Instability to Enhance Dynamic Power Limit of Turbines and Compressors," United States Patent 4,273,510, June 1981.

7. Von Pragenau, G.L., "Damping Seals for Turbomachinery," NASA TP-1987, 1982.

8. Miller, E.H., "Rotor Stabilizing Labyrinth Seal for Steam Turbines," United States Patent 4,420,161, Dec. 1983.

9. Wyssmann, H.R., Sulzer Escher Wyss, Sulzer Symposium for Rotating Equipment Specialists, Scottsdale, AZ, Jan. 26-27, 1984.

10. Wyssmann, H.R., "Theory and Measurements of Labyrinth Seal Coefficients for Rotor Stability of Turbocompressors," Rotordynamic Instability Problems in High-Performance Turbomachinery - 1986, NASA CP-2443, D.W. Childs, J.M. Vance, and R.C. Hendricks, eds., NASA, 1986, pp. 237-258.

11. Brown, R.D., and Hart, A., "A Novel Form of Damper for Turbo-machinery," Rotordynamic Instability Problems in High-Performance Turbomachninery - 1986, NASA CP-2443, D.W. Childs, J.M. Vance, and R.C. Hendricks, eds., NASA, 1986, pp. 325-348.

12. Iwatsubo, T., ed.: Post International Federation Theory of Mechanics and Mechanisms IFToMM Conference on Flow Induced Force in Rotating Machinery, Proceedings, Kobe University, Japan, Sept. 1986.

13. Braun, M.J., Batur, C., Ida, N., Rose, B., Hendricks, R.C., and Mullen, R.L., "A Non-Invasive Laser Based Analysis for Thin Film Flows at Low Reynolds Numbers," International Conference on Tribology Lubrication and Wear, Institute of Mechanical Engineers, London, UK, July 1-3, 1987, Paper No. 342/143,

14. Mullen, R.L., and Hendricks, R.C., "Finite Element Formulation for Transient Heat Treat Problems," ASME-JSME Thermal Engineering Joint Conference, Vol. 3, Y. Mori and W.J. Yung, eds., ASME, New York, 1983, pp. 367-374. (NASA TM-83070.)

15. Tam, L.T., "An Interim Report on the Calculation Method for a Multi-Dimensional Whirling Seal," CHAM of North America, Huntsville, AL, 1985.

16. Tam, L.T., Przekwas, A.J., and Hendricks, R.C., "Numerical Modelling of Multi-Dimensional Whirling Seal and Bearings," NASA Lewis Research Center, Dec. 1986.

17. Launder, B.E., and Spalding D.B., "The Numerical Computation of Turbulent Flows," Computer Methods in Applied Mechanics and Engineering, Vol. 3, No. 2, Mar. 1974, pp. 269-289.

18. Spalding, D.B., "A General Purpose Computer Program for Multi-Dimensional One- and Two-Phase Flow," Mathematics and Computers in Simulation, Vol. 23, No. 3, Sept. 1981, pp. 267-276.

19. Childs, D.W., "The SSME HPFTP Interstage Seals: Analysis and Experiments for Leakage and Reaction Force Coefficients," NASA CR-170876, 1983..

20. Muszynska, A., "Model Testing of Rotor/Bearing Systems," The International Journal of Analytical and Experimental Modal Analysis, Vol. 1, No. 3, 1986.

21. Muszynska, A., "Fluid-Related Rotor/Bearing/Seal Instability Problems," Bently Rotor Dynamics Research Corporation, Minden, NV, 1986.

22. Muszynska, A., "Whirl and Whip-Rotor/Bearing Stability Problems," Journal of Sound and Vibration, Vol. 110, No. 3, Nov. 8, 1986, pp. 443-462.

23. Bolotin, V.V., and Weingarten, V.I., Non-conservative Problems in Elastic Stability Theory (in Russian), Gos. Isd. Fiz. Mat. Lit., Moskva 1961.

24. Black, H.F., "Effects of Hydraulic Forces in Annular Pressure Seals on the Vibrations of Centrifugal Pump Rotors," Journal of Mechanical Engineering Science, Vol. 11, No. 2, Apr. 1969, pp. 206-213.

25. Black, H.F., and Jenssen, D.N., "Dynamic Hybrid Bearing Characteristics of Annular Controller Leakage Seals," Proceedings of Institution of Mechanical Engineers, Vol. 184, Pt. 3N, 1969-1970, pp. 92-100.

26. Muszynska, A., "Improvements in Lightly Loaded Rotor/Bearing and Rotor/Seal Models," Presented at the ASME Conference on Vibration and Noise, Boston, MA, Sept. 1987.

TABLE I. – NUMERICAL PARAMETERS FOR SEAL/BEARING CALCULATIONS (CASES 1 TO 8)

Case	Average inlet pressure, P_{in}, bar	Pressure outlet pressure, P_{out}, bar	Average pressure drop, Δ_p, bar	Ratio of precession amplitude to radial clearance, A/c	Rotative speed, ω_R, rpm	Ratio of precession freqency to rotative speed, ω_p/ω_R	Preswirl	Injection rate, kg/sec	Calculated total average leakage, kg/sec		Axial force, F_z, N	Case illustrated in figure-
									Low ω_R	High ω_R		
1a 1b	69.7 63.1	66 44.4	3.7 18.5	0.24	1442 2344 3252 4181 5085	1	No	0	3.37 7.54	3.05 (for 1a) 7.58 (for 1b)	57.4 287.2	3 ------
2	62.5	45.5	17	0.5	1442 3252 5085	0.3 .5 .75 1	No	0	7.48 7.49	7.41 (low ω_p/ω_R) 7.49 (high ω_p/ω_R)	----- 263.8	4 to 6 ------
3	62.5	45.5	17	0.24	1442 3252 5085	0.5 .75 1	No	0	7.34 7.38	7.26 (low ω_p/ω_R) 7.32 (high ω_p/ω_R).	49.7 263.4	6,7 ------
4a 4b	69.7 62.5	66.5 45.5	3.2 17	0.24	1442 2344 3252 4181 5085	1	Yes	0	3.21 7.38	2.84 (for 4a) 7.32 (for 4b)	49.7 263.4	8 to 10 -------
5	69.07	69.57	0.5	0.8	1442 2344 3252 4181 5085	1	No	$\frac{\omega_R}{15\ 352}$	1.17 1.17 1.17	1.47 (with rotation) 1.43 (radial) 1.37 (against rotation)	7.8 ---- ----	------- 12, 13 14
6	69.5	69.2	0.3	0.24	1442 3252 5085	0.15 .5 .8	No	0	0.80 .82	0.63 (low ω_p/ω_R) .78 (high ω_p/ω_R)	---- 4.7	15 ------
7	0	0	0	0.983	60	1	No	0	----	----------	0	16
8	1.1	1	0.1	0.983	60	1	No	0	----	----------	1.6	17

TABLE II. - FLUID PROPERTIES USED IN NUMERICAL CALCULATIONS

Fluid	Density, ρ, kg/m^3	Kinematic viscosity, ν, m^2/s	Cases
Bromotri-fluoromethane	1570	10^{-7}	1 to 6
Oil	800	6×10^{-5}	7 and 8

TABLE III. - GEOMETRIC PARAMETERS USED IN NUMERICAL CALCULATIONS

Parameter	Fluid	
	Bromotri-fluoromethane	Oil
Seal or bearing length, ℓ, m	48.29×10^{-3}	76.2×10^{-3}
Shaft radius, R_i, m	49.6528×10^{-3}	38.1×10^{-3}
Seal or bearing radius, R, m	50.1478×10^{-3}	76.2×10^{-3}
Radial clearance c, m	495×10^{-6}	38.1×10^{-3}
Ratio of clearance to shaft radius, c/R_i	9.8×10^{-3}	1

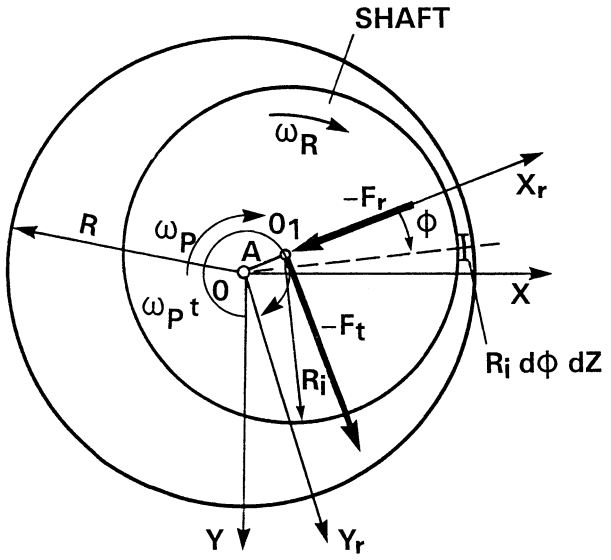

FIGURE 1. - SEAL OR BEARING CONFIGURATION IN A CONSTANT AXIAL PLANE Z.

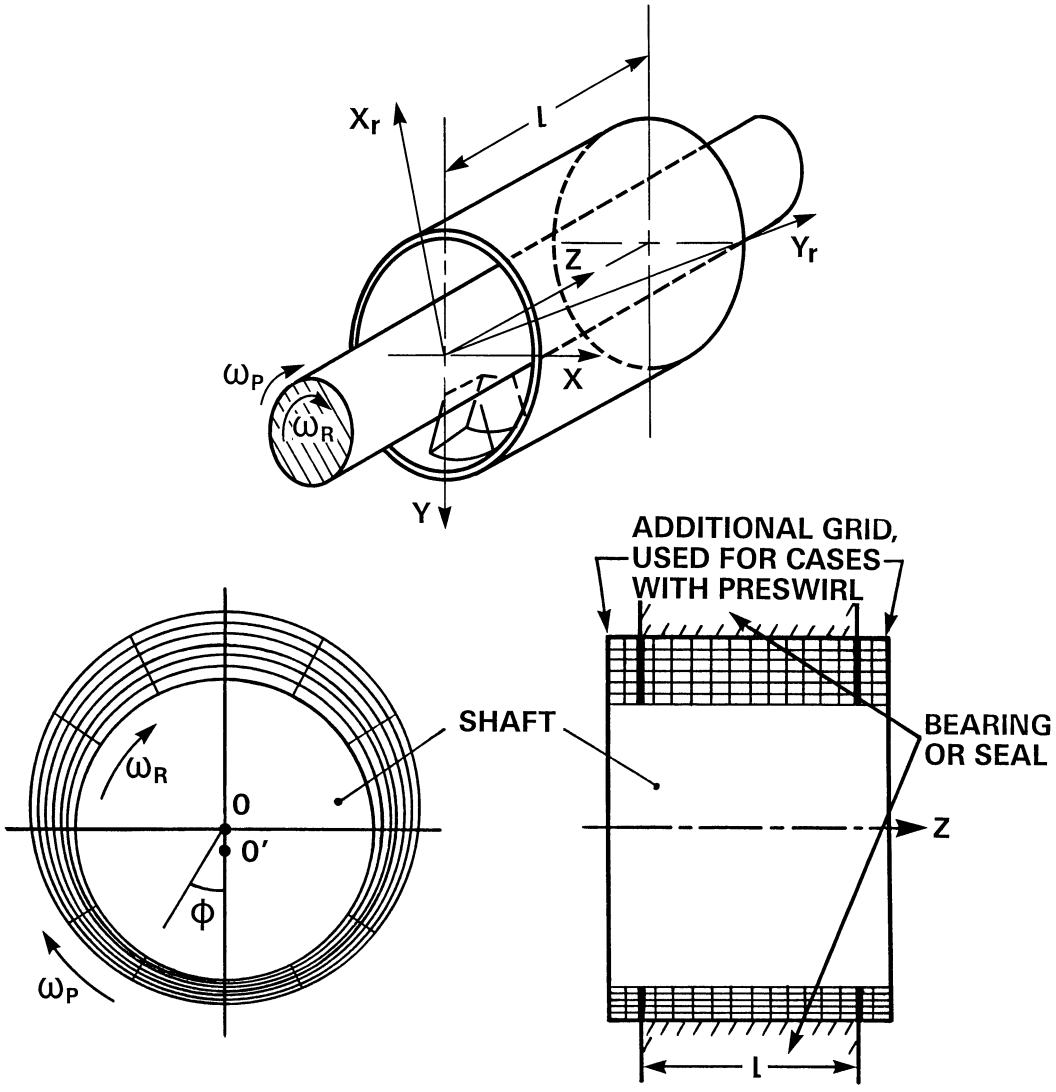

FIGURE 2. - SHAFT/HOUSING CONFIGURATION AND FLUID FLOW GRID DISTRIBUTION.

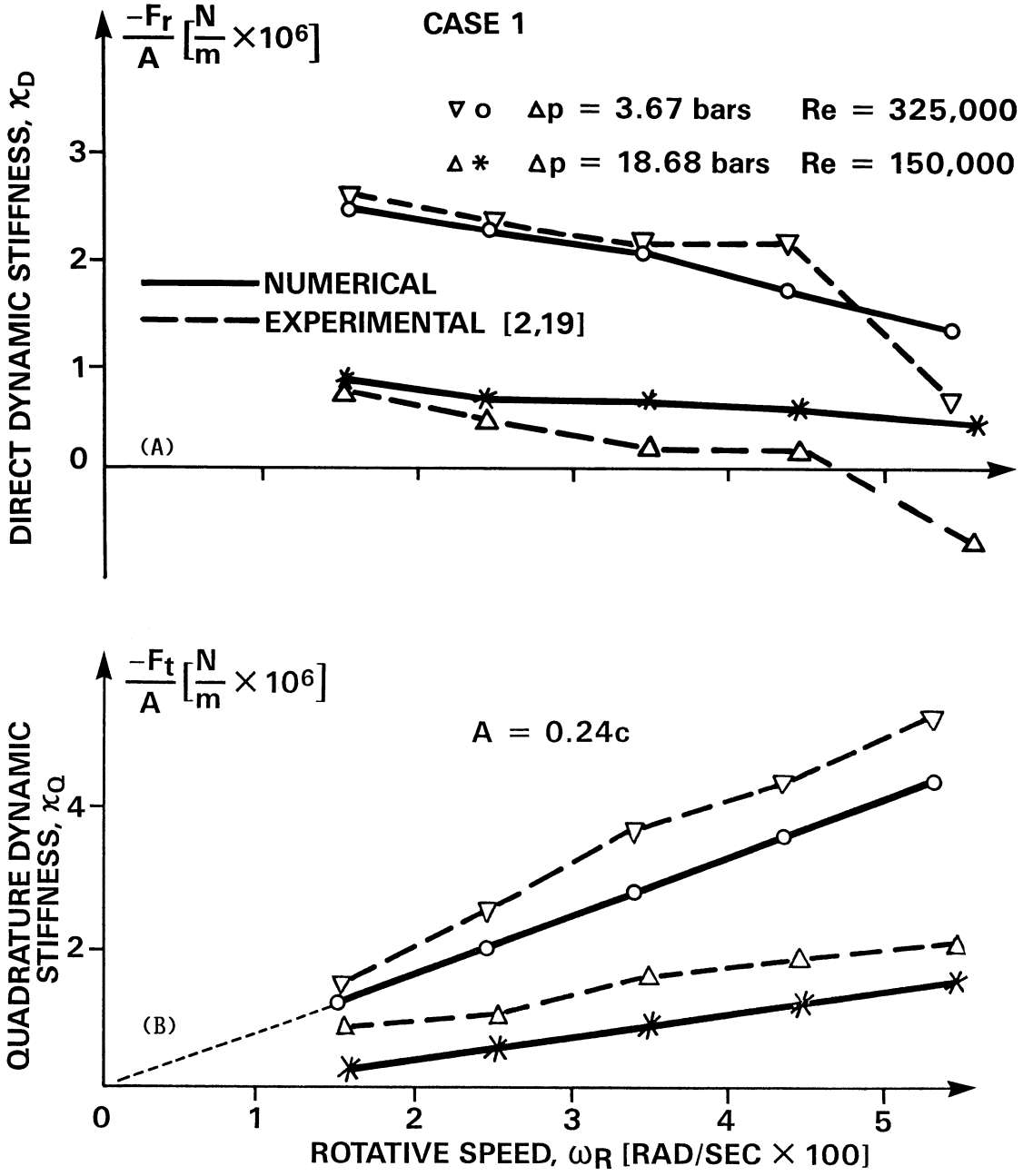

FIGURE 3. - FLUID DIRECT AND QUADRATURE DYNAMIC STIFFNESSES VERSUS ROTOR SPEED FOR TWO AXIAL REYNOLDS NUMBERS. A COMPARISON OF CALCULATIONS AND MEASUREMENTS BY CHILDS [2, 19].

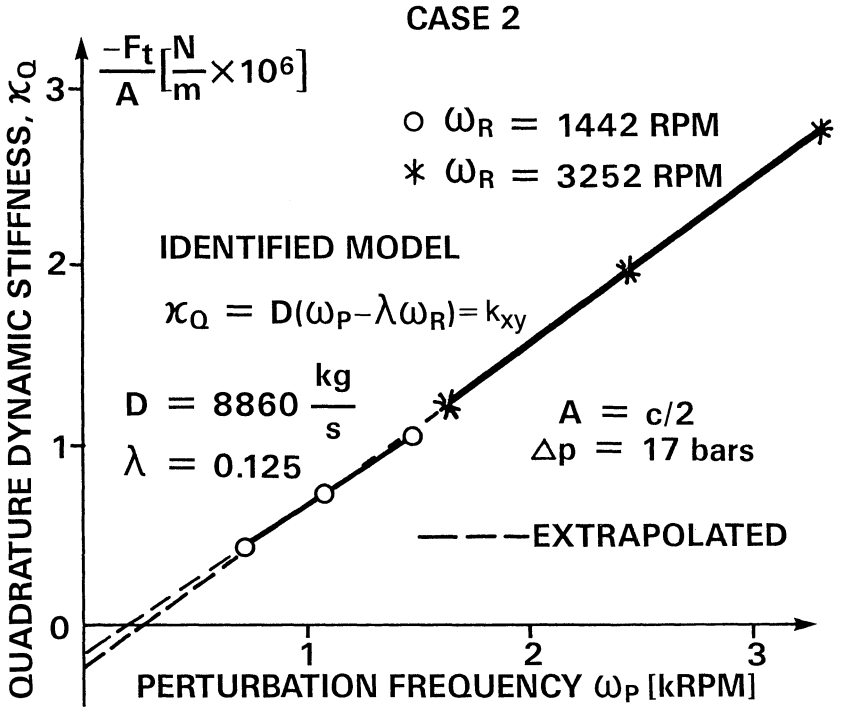

FIGURE 4. - QUADRATURE DYNAMIC STIFFNESS VERSUS PERTURBATION FREQUENCY. IDENTIFICATION OF FLUID RADIAL DAMPING D AND FLUID AVERAGE CIRCUMFERENTIAL VELOCITY RATIO λ.

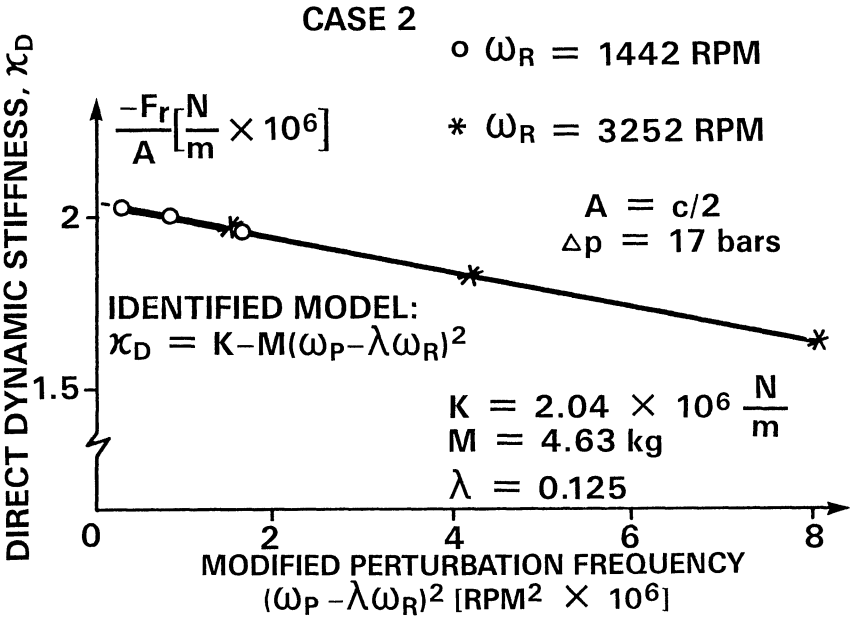

FIGURE 5. - DIRECT DYNAMIC STIFFNESS VERSUS MODIFIED PERTURBATION FREQUENCY. IDENTIFICATION OF FLUID RADIAL STIFFNESS K AND FLUID INERTIA M.

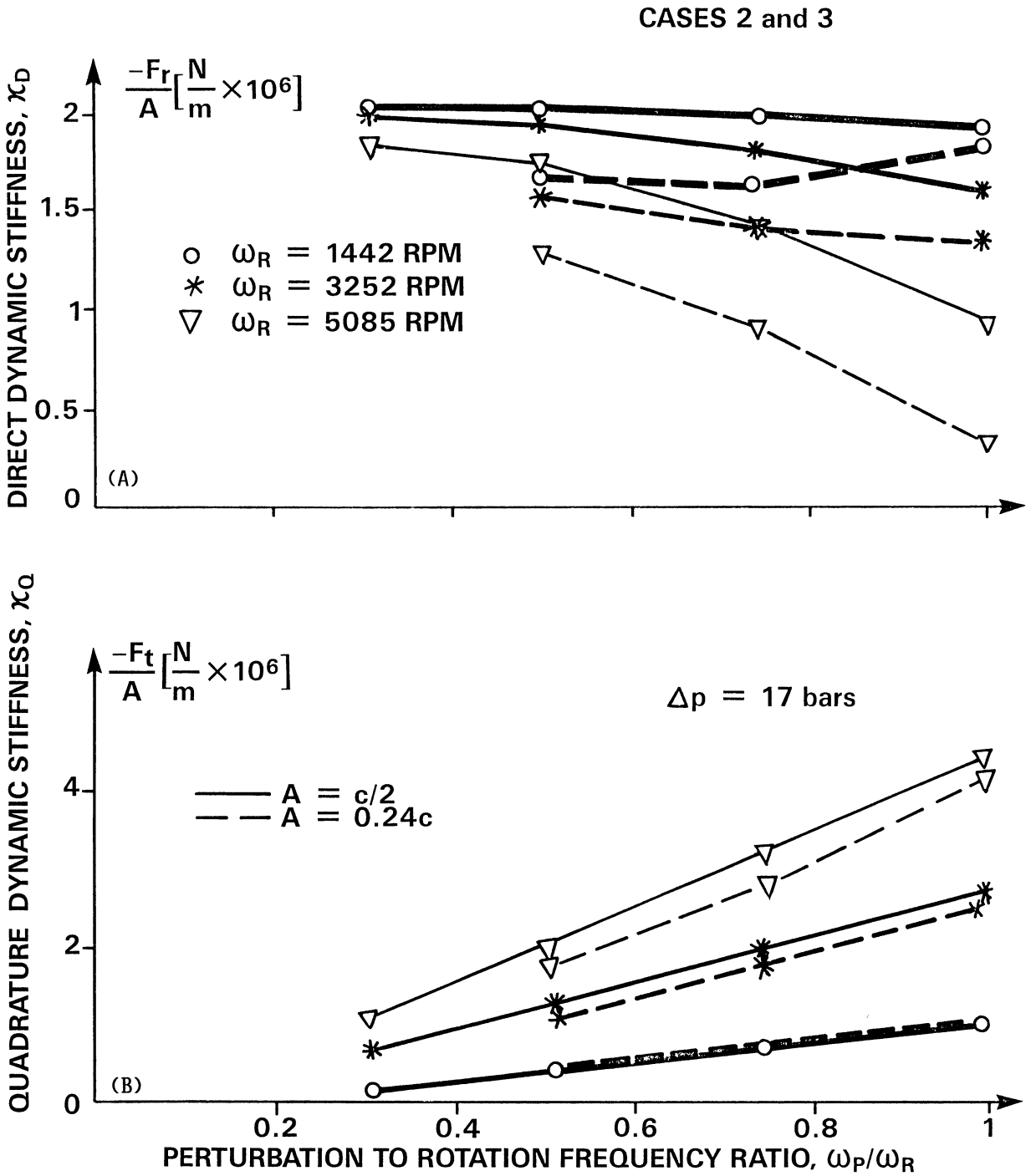

FIGURE 6. - DIRECT AND QUADRATURE DYNAMIC STIFFNESSES VERSUS RATIO OF PERTURBATION TO ROTATION FREQUENCY FOR A = 0.5c AND A = 0.24c. EFFECT OF NONLINEARITY.

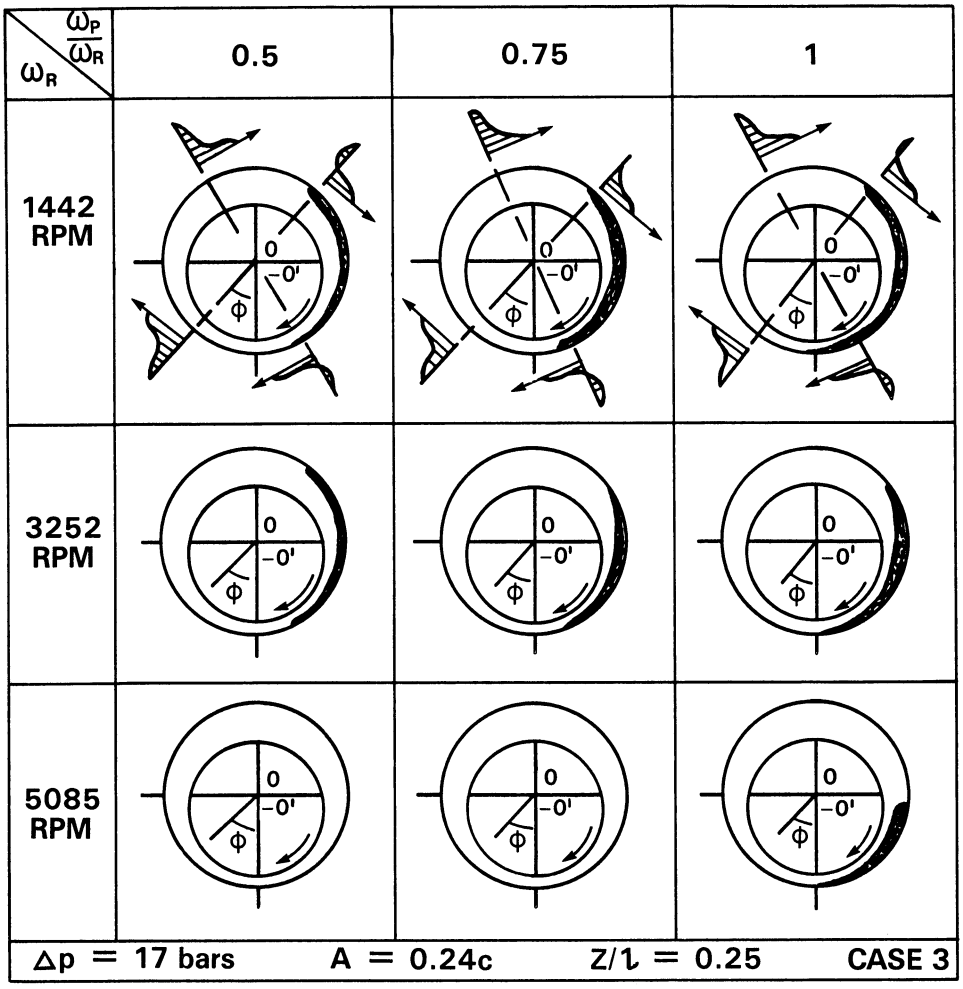

FIGURE 7. - INFLUENCE OF ROTATION AND PERTURBATION SPEED ON SECONDARY FLOW PATTERNS (SHADOWED AREAS) IN SEAL FLOWS.

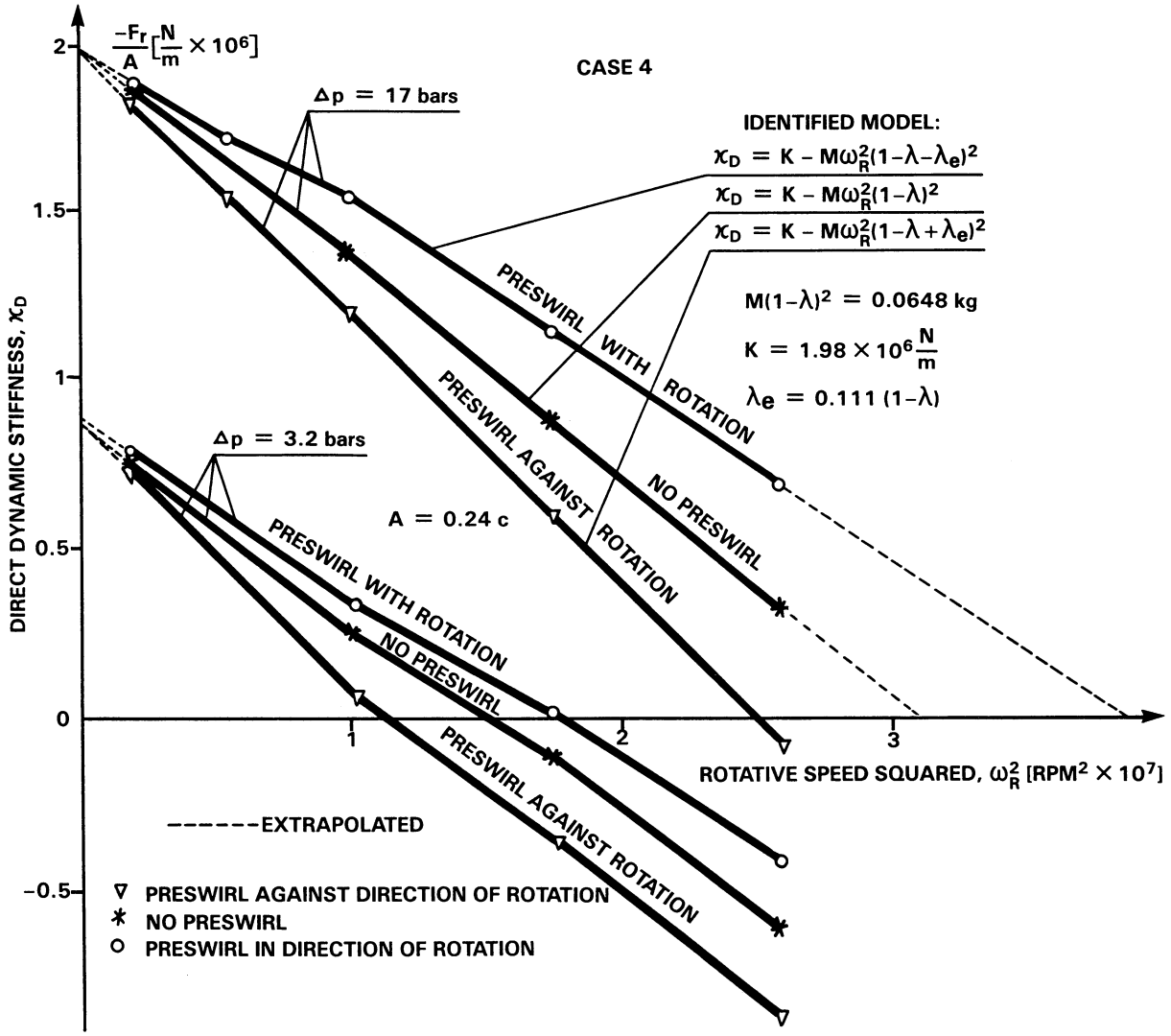

FIGURE 8. - DIRECT DYNAMIC STIFFNESS VERSUS ROTATIVE SPEED SQUARED (SYNCHRONOUS PERTURBATION). NOTE INFLUENCE OF PRESWIRL ON AVERAGE CIRCUMFERENTIAL VELOCITY RATIO.

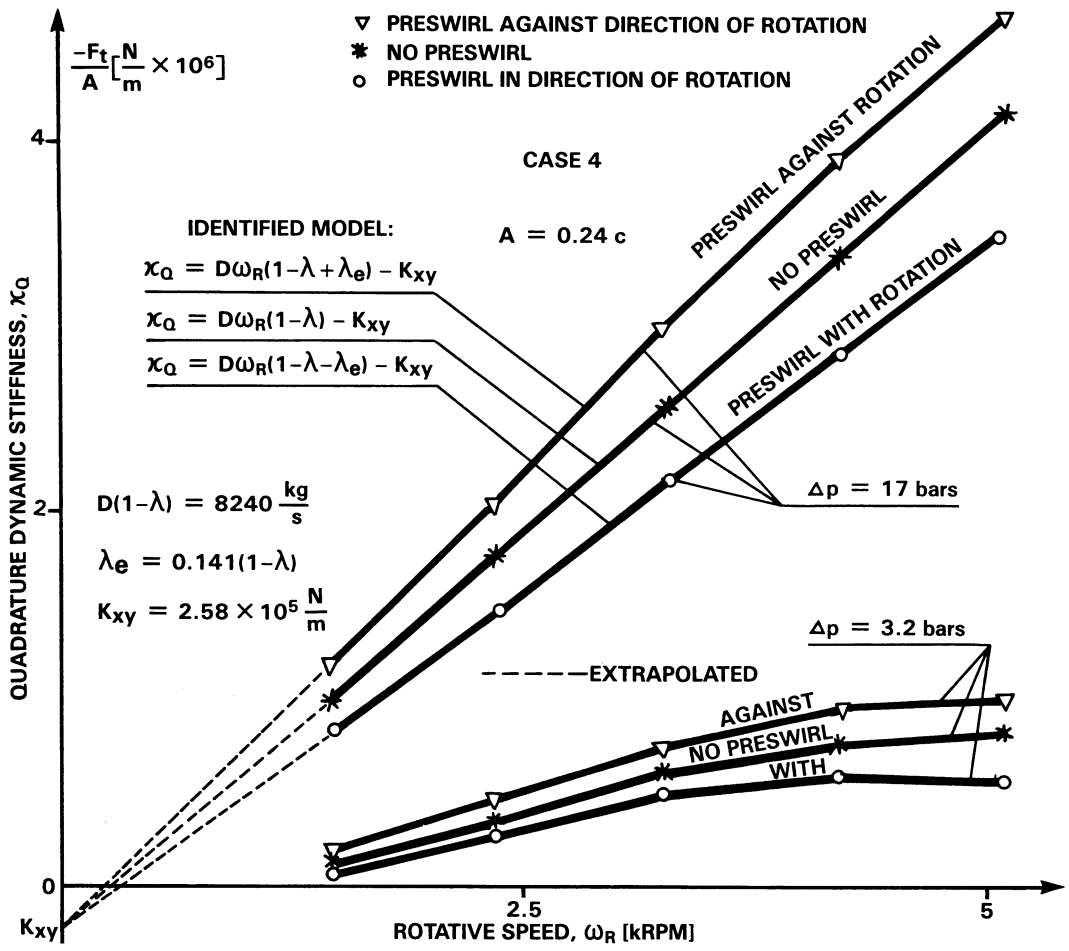

FIGURE 9. - QUADRATURE DYNAMIC STIFFNESS VERSUS ROTATIVE SPEED (SYNCHRONOUS PERTURBATION). NOTE INFLUENCE OF PRESWIRL ON AVERAGE CIRCUMFERENTIAL VELOCITY RATIO.

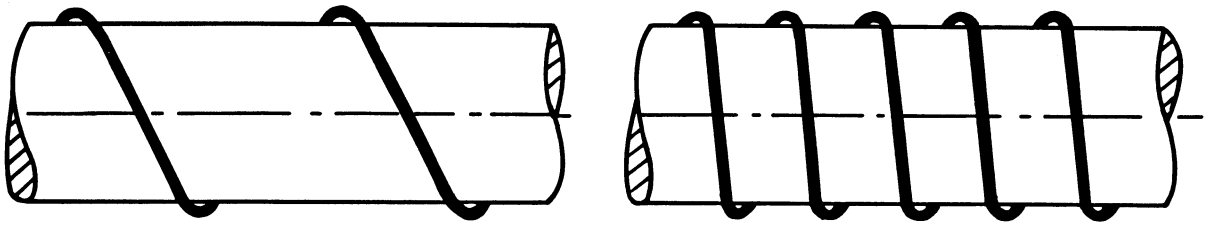

(A) HIGH PRESSURE DROP. (B) LOW PRESSURE DROP.

FIGURE 10. - INTERPRETATION OF AXIAL AND CIRCUMFERENTIAL FLOW RESULTING IN "SPIRAL" FLOW.

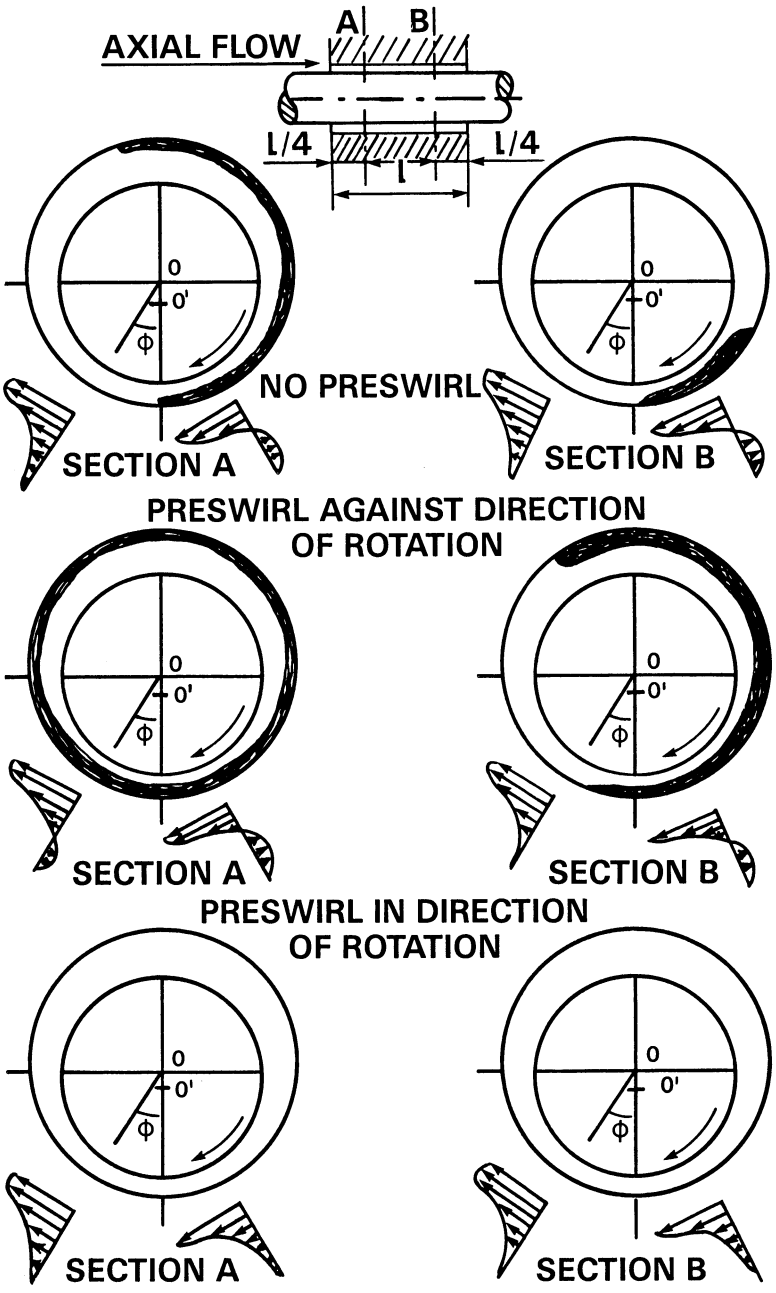

FIGURE 11. - INFLUENCE OF PRESWIRL ON CIRCUMFERENTIAL FLOW FIELD. SHADOWED AREAS INDICATE SECONDARY FLOWS.

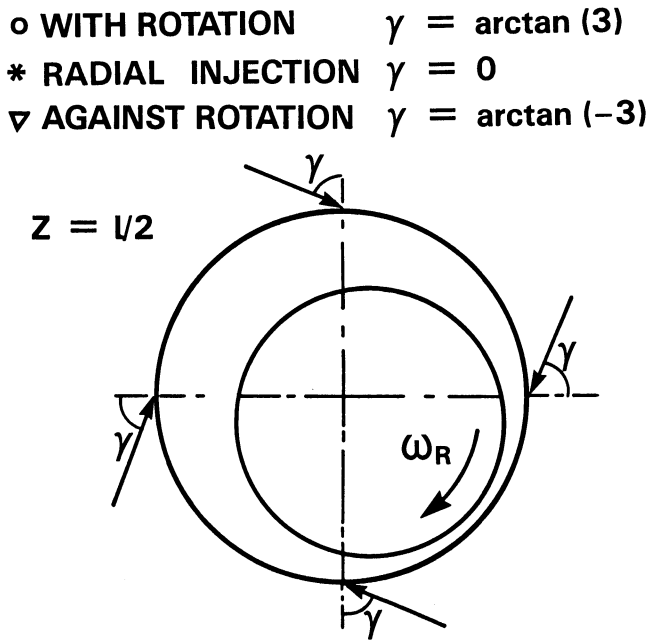

FIGURE 12. - INJECTION GEOMETRY.

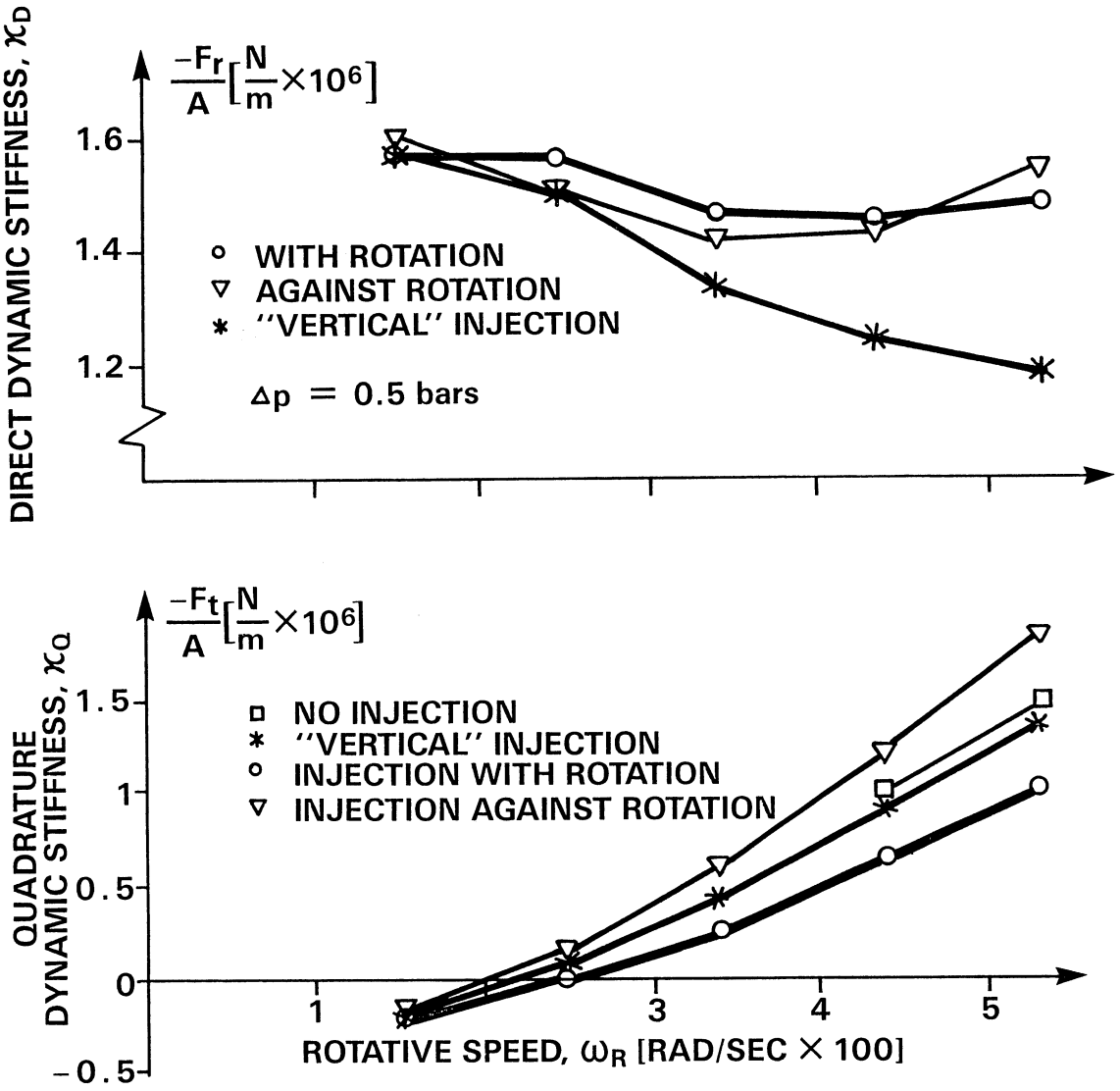

FIGURE 13. - DIRECT AND QUADRATURE DYNAMIC STIFFNESSES VERSUS ROTATIVE SPEED FOR CASES WITH FLUID INJECTION (SYNCHRONOUS PERTURBATION).

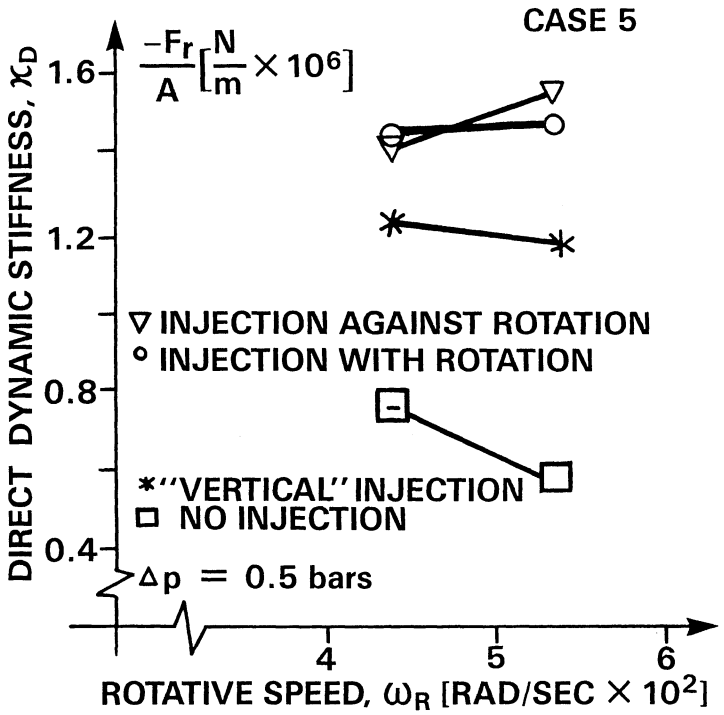

FIGURE 14. - DIRECT DYNAMIC STIFFNESS VERSUS ROTATIVE SPEED FOR CASES WITH AND WITHOUT FLUID INJECTION (DIFFERENT SCALE THAN IN FIG. 13).

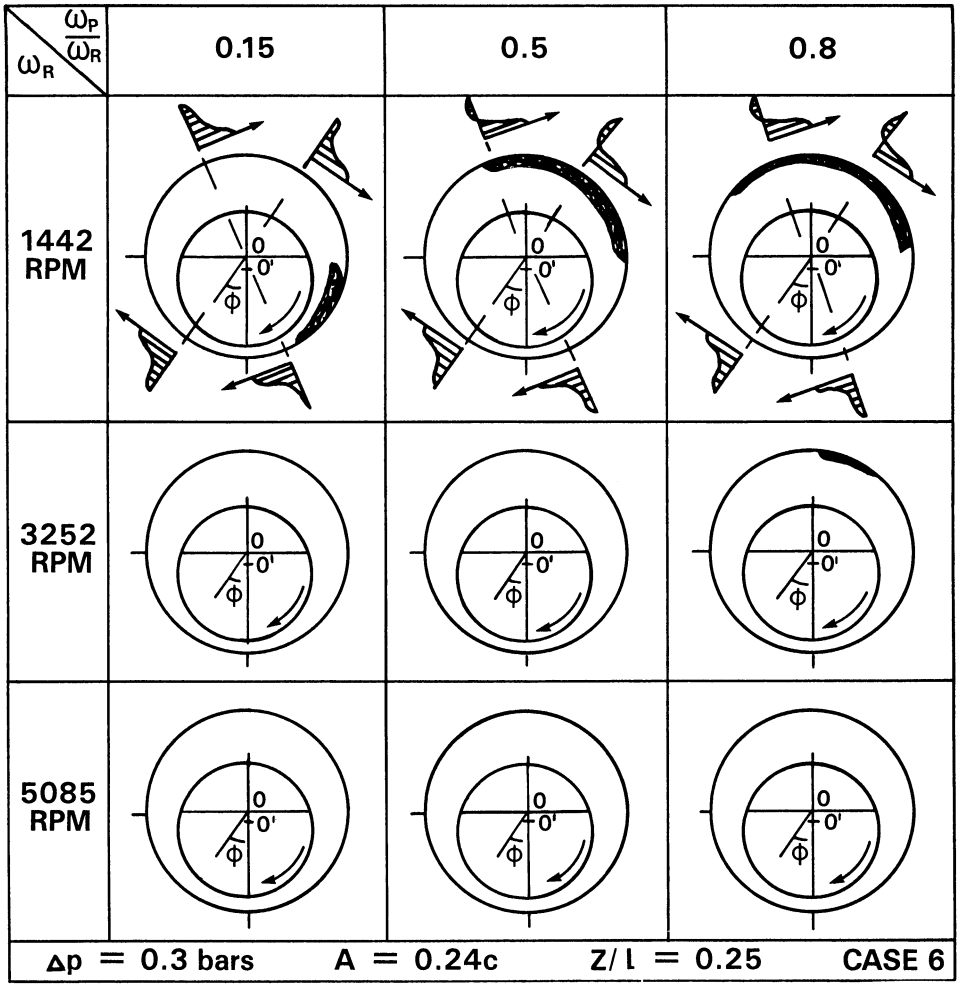

FIGURE 15. - INFLUENCE OF ROTATION AND PERTURBATION SPEED ON SECONDARY FLOW PATTERNS (SHADOWED AREAS) IN BEARING FLOWS. COMPARE WITH FIGURE 7.

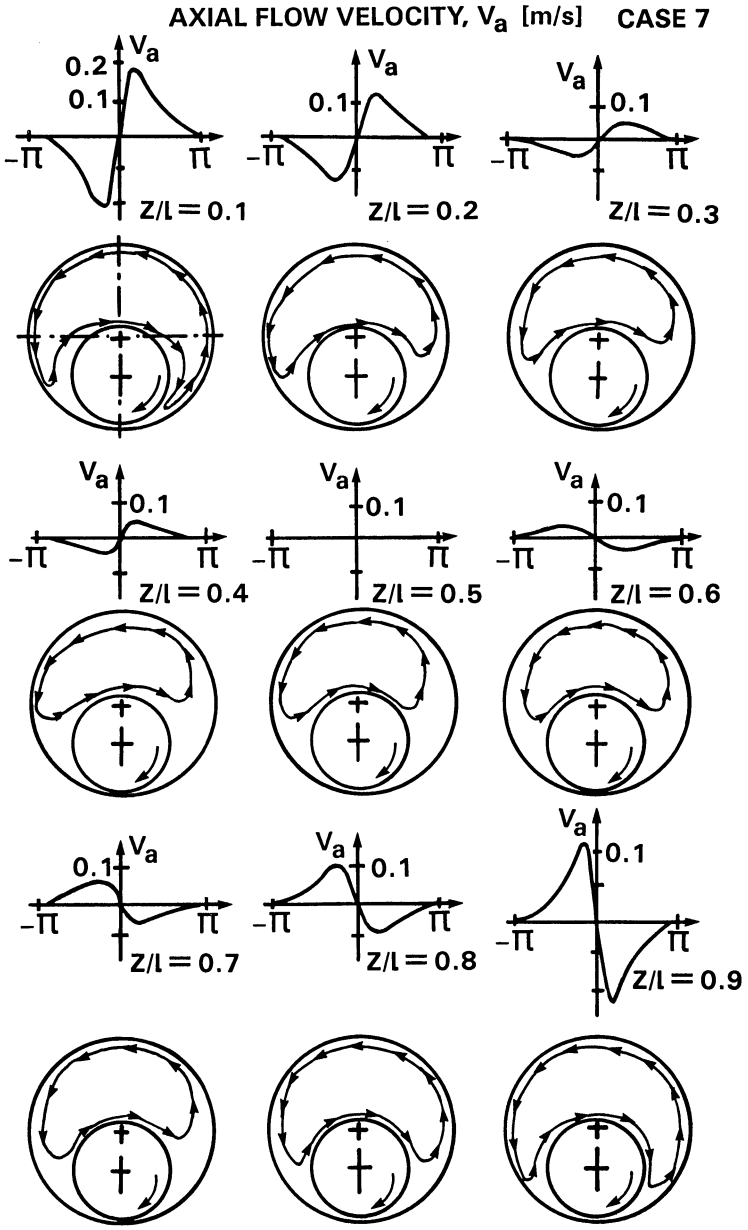

FIGURE 16. - MEAN AXIAL FLOW DISTRIBUTION ALONG UNWRAPPED CIRCUMFERENTIAL DIRECTION AND SECONDARY FLOW PATTERNS OF A BEARING AT VARIOUS AXIAL PLANES. PRESSURE DROP Δp = 0 BAR, (ω_p = 0).

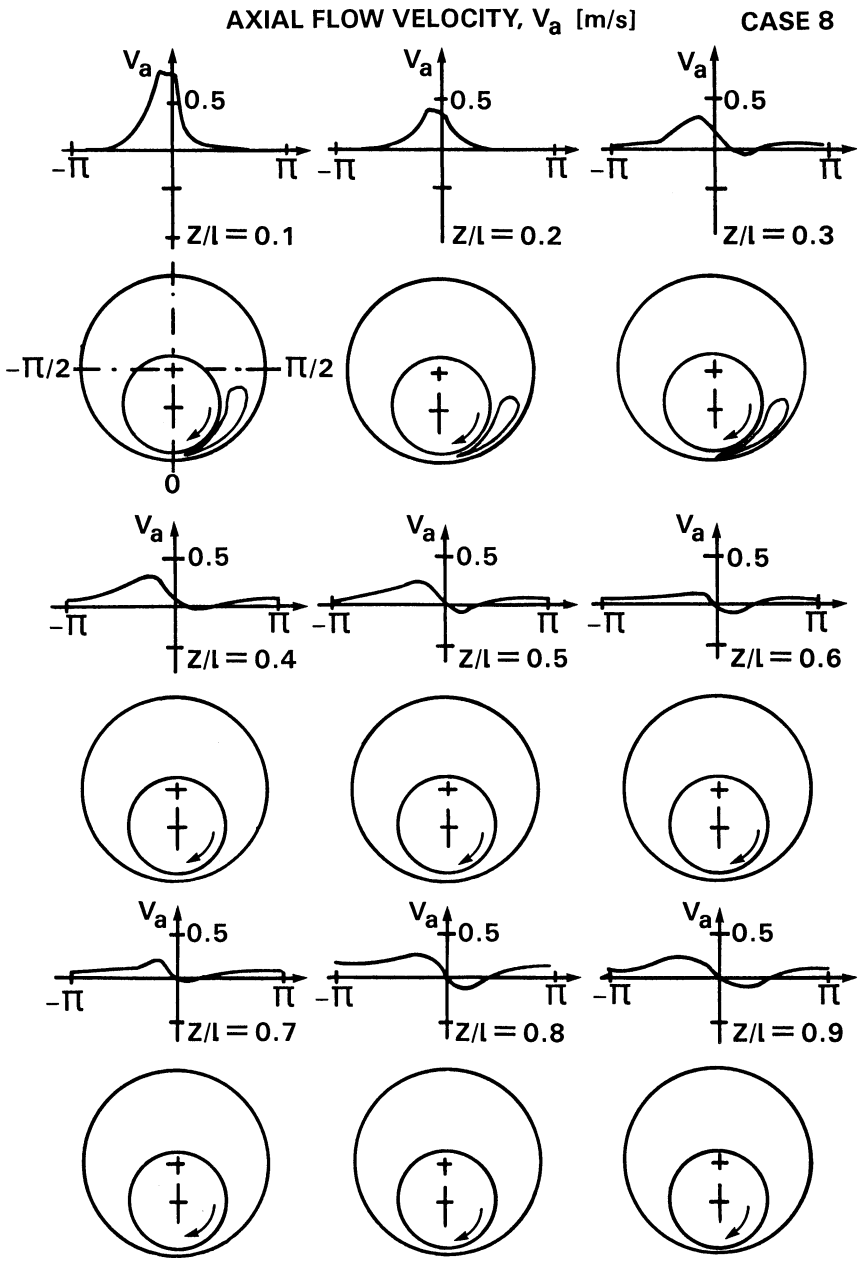

FIGURE 17. - MEAN AXIAL FLOW DISTRIBUTION ALONG UNWRAPPED CIRCUMFERENTIAL DIRECTION AND SECONDARY FLOW PATTERNS OF A BEARING AT VARIOUS AXIAL PLANES. PRESSURE DROP Δp = 0.1 BAR, (ω_p = 0).

NASA
National Aeronautics and Space Administration

Report Documentation Page

1. Report No.	2. Government Accession No.	3. Recipient's Catalog No.
NASA TM-100268		

4. Title and Subtitle

Numerical and Analytical Study of Fluid Dynamic Forces in Seals and Bearings

5. Report Date

6. Performing Organization Code

7. Author(s)

L.T. Tam, A.J. Przekwas, A. Muszynska, R.C. Hendricks, M.J. Braun, and R.L. Mullen

8. Performing Organization Report No.

E-3903

10. Work Unit No.

505-62-21

9. Performing Organization Name and Address

National Aeronautics and Space Administration
Lewis Research Center
Cleveland, Ohio 44135-3191

11. Contract or Grant No.

13. Type of Report and Period Covered

Technical Memorandum

12. Sponsoring Agency Name and Address

National Aeronautics and Space Administration
Washington, D.C. 20546-0001

14. Sponsoring Agency Code

15. Supplementary Notes

Prepared for the 11th Biennial Design Engineering Conference on Vibration and Noise sponsored by the American Society of Mechanical Engineers, Boston, Massachusetts, September 27-30, 1987. L.T. Tam and A.J. Przekwas, CHAM of North America, Inc., Huntsville, Alabama 35816; A. Muszynska, Bently Rotor Dynamics Research Corporation, Minden, Nevada 89423; R.C. Hendricks, NASA Lewis Research Center; M.J. Braun, University of Akron, Akron, Ohio 44325; R.L. Mullen, Case Western Reserve University, Cleveland, Ohio 44106.

16. Abstract

A numerical model based on a transformed, conservative form of the three-dimensional Navier-Stokes equation and an analytical model based on "lumped" fluid parameters are presented and compared with studies of modeled rotor bearing/seal systems. The rotor destabilizing factors are related to the rotative character of the flow field. It is shown that these destabilizing factors can be reduced through a decrease in the fluid average circumferential velocity. However, the rotative character of the flow field is a complex three-dimensional system with bifurcated secondary flow patterns that significantly alter the fluid circumferential velocity. By transforming the Navier-Stokes equations to those for a rotating observer and using the numerical code PHOENICS-84 with a nonorthogonal body-fitted grid, several numerical experiments were carried out to demonstrate the character of this complex flow field. In general, fluid injection and/or preswirl of the flow field opposing the shaft rotation significantly intensified these secondary recirculation zones and thus reduced the average circumferential velocity; injection or preswirl in the direction of rotation significantly weakened these zones. A decrease in average circumferential velocity was related to an increase in the strength of the recirculation zones and thereby promoted stability. The influence of the axial flow was analyzed. The lumped model of fluid dynamic force based on the average circumferential velocity ratio (as opposed to the bearing/seal coefficient model) well described the obtained results for relatively large but limited ranges of parameters. This lumped model is extremely useful in rotor bearing/seal system dynamic analysis and should be widely recommended. Fluid dynamic forces and leakage rates were calculated and compared with seal data where the working fluid was bromotrifluoromethane ($CBrF_3$). The radial and tangential force predictions were in reasonable agreement with selected experimental data. Nonsynchronous perturbation provided meaningful information for system lumped-parameter identification from numerical experiment data.

17. Key Words (Suggested by Author(s))	18. Distribution Statement
Seals; Numerical; Fluid dynamics; Forces; Bearings; Stability	Unclassified - Unlimited Subject Category 34

19. Security Classif. (of this report)	20. Security Classif. (of this page)	21. No of pages	22. Price*
Unclassified	Unclassified	38	A03

*For sale by the National Technical Information Service, Springfield, Virginia 22161